Atmos. Meas. Tech. Discuss., doi:10.5194/amt-2015-361, 2016
Manuscript under review for journal Atmos. Meas. Tech.
Published: 21 January 2016

Atmospheric Measurement Techniques Discussions

Direct assimilation of Chinese FY-3C Microwave Temperature Sounder-2 radiances in the global GRAPES system

J.LI[1,2] and G. Liu[1,2]

[1] National Meteorological Center, China Meteorological Administration, Beijing, 100081, China

[2] Numerical Weather Prediction Center, China Meteorological Administration, Beijing, 100081, China

Correspondence to: J. Li (lj@cma.gov.cn)

Abstract

FengYun-3C (FY-3C) is an operational polar-orbiting satellite carrying the new-generation microwave sounding instruments in China. This paper describes the assimilation of the FY-3C Microwave Temperature Sounder-2 (MWTS-2) radiances in the Global and Regional Assimilation and PrEdiction System (GRAPES) of China Meteoroligcal Administration. A quality control (QC) procedure for the assimilation of MWTS-2 radiance is proposed. Extensive monitoring before assimilation shows that MWTS-2 observations exhibit a clear striping pattern. A technique combining principal component analysis (PCA) and Ensemble Empirical Mode Decomposition (EEMD) is applied to the observations to remove the striping noise. Cloudy field-of-views (FOVs) are identified by applying the Visible and InfrarRed Radiometer (VIRR) cloud fraction threshold of 76%. Other QC steps include the following: (i) eight outmost FOVs, (ii) channel 6 if the terrain altitude is greater than 500 m, (iii) channel 5 over sea ice and land, (iv) coastal FOVs, and (v) outliers with large differences between observations and model simulations. Approximately 83%, 75%, 40% and 40% of the observations are removed by the proposed QC for channels 5-8, respectively. After QC, the global biases and standard deviations are reduced significantly. The assimilation of the MWTS-2 radiances shows a positive impact when the control experiment assimilates only conventional observations. The experiments also show that the analysis and forecast errors are

Atmos. Meas. Tech. Discuss., doi:10.5194/amt-2015-361, 2016
Manuscript under review for journal Atmos. Meas. Tech.
Published: 21 January 2016

Atmospheric Measurement Techniques Discussions

slightly reduced when the striping noise is removed from the observations. The quality control scheme of extracting the striping noise may contribute to the analysis and forecast. The impact of MWTS-2 is neutral when the conventional data and other satellite data are all assimilated.

1 Introduction

Satellite radiance data have become a critical component in the Numerical Weather Prediction (NWP) system. It is widely accepted that direct assimilation of observations from microwave temperature sounding channels can significantly improve the accuracy of global and regional weather analysis and forecasts (Andersson et al., 1994; Courtier et al., 1998; Derber and Wu, 1998; McNally et al., 2000; Kozo et al., 2005). Most NWP centers, which made effective early use of ATOVS (Advanced TIROS [Television and Infrared Observational Satellite] Operational Vertical Sounder), onboard NOAA (National Oceanic and Atmospheric Administration)-15/16/17/18/19, MetOp (The Meteorological Operational satellite A)-A/B and Aqua, have reported a substantial reduction in the forecast root mean square (RMS) error. Adjoint-based estimates of observation impact on NWP (Baker and Daley, 2000) have further demonstrated that the greatest decrease in forecast error is due to Advanced Microwave Sounding Unit-A (AMSU-A), which was launched as part of ATOVS and is used primarily for global atmospheric temperature sounding (Fourrié et al., 2002; Langland and Baker, 2004; Cardinali, 2009; Gelaro et al., 2010). Observations from Microwave Temperature Sounder-1 (MWTS-1) onboard Fengyun-3A (FY-3A) and Fengyun-3B (FY-3B) have positive impacts on NWP forecasts (Lu et al., 2010; Lu and Bell, 2012; Li and Zou, 2013, 2014; Li and Liu, 2015).

On September 23, 2013, the Fengyun-3C (FY-3C) satellite was launched successfully with 11 more advanced instruments on board. It is an operational polar-orbiting environmental research satellite. FY-3C has an afternoon configuration with a local equator crossing time (ECT) of approximately 10 AM. Of particular interest for NWP data assimilation is Microwave Temperature Sounder-2 (MWTS-2) and Microwave Humidity Sounder-2 (MWHS-2). An evaluation of FY-3C satellite data quality has beed done by Lu et al. (Lu et al., 2015). In this thesis, the assimilaiton of MWTS-2 will be introduced. After the intensive calibration/validation period in its first 6 months in orbit, the performance of atmospheric sounding instruments in particular meets or exceeds the specifications.

Atmos. Meas. Tech. Discuss., doi:10.5194/amt-2015-361, 2016
Manuscript under review for journal Atmos. Meas. Tech.
Published: 21 January 2016

Atmospheric Measurement Techniques Discussions

MWTS-2 is more advanced than MWTS-1 onboard FY-3A/B (Dong et al., 2009; Zhang et al., 2009). The spectral resolution of MWTS-2 is much higher than that of MWTS-1. It has 13 channels for atmospheric temperature profiling from the Earth's surface to 1 hPa above, whereas MWTS-1 only has four channels. The spatial resolution of MWTS-2 is also much higher than MWTS-1. There are 90 scene fields of view (FOVs) in each scan line for MWTS-2, whereas MWTS-1 has only 15 FOVs. Compared with AMSU-A, MWTS-2 has more channels at approximately 50-60 GHz and more FOVs on a cross-track scan line for all channels. AMSU-A has only 30 FOVs on each scan line. The spatial resolution of MWTS-2 is three times that of AMSU-A. MWTS-2 can provide a temperature structure with higher vertical and spatial resolution than MWTS-1 and AMSU-A. Compared with the Advanced Technology Microwave Sounder (ATMS) onboard the Suomi National Polar-orbiting Partnership (SNPP), the channel specifications of MWTS-2 onboard FY-3C are similar in the 50-60 GHz oxygen line. However, FY-3C is a morning satellite and ATMS is an afternoon satellite. They observe different regions of the earth simultaneously. The MWTS-2 observations can be complementary to ATMS observations. The FY-3C will significantly contribute to the Global Environmental Observing System of Systems (GEOSS).

The assimilations of AMSU-A and ATMS radiance observations have been demonstrated to have a significantly positive impact on the NWP forecast (Derber and Wu, 1998; Cardinali, 2009; Zou and Weng, 2013). Furthermore, research has also shown that the assimilation of FY-3A and FY-3B microwave temperature radiance can improve NWP analyses and forecasts (Li and Zou, 2013, 2014; Li and Liu, 2015). In fact, MWTS-2 is more advanced than MWTS-1. The sounding abilities are comparable with those of ATMS and are much better than those of AMSU-A. It is anticipated that the MWTS-2 data could also be useful for NWP modeling systems if properly assimilated.

The aim of this study was to assimilate, for the first time, FY-3C MWTS-2 radiance data into the Global and Regional Assimilation and PrEdiction System (GRAPES) of China Meteorological Administration (CMA) (Chen et al., 2008; Xue and Chen, 2008, Xue et al., 2008). In this research, the observation processing and quality control (QC) for FY-3C radiance will be developed. The impact of FY-3C MWTS-2 on the GRAPES assimilation system will be evaluated.

This paper is organized as follows. Section 2 describes the general details of the FY-3C MWTS-2 radiance data. Section 3 describes the GRAPES three-dimensional variational

Atmos. Meas. Tech. Discuss., doi:10.5194/amt-2015-361, 2016
Manuscript under review for journal Atmos. Meas. Tech.
Published: 21 January 2016

Atmospheric Measurement Techniques Discussions

assimilation (3D-Var) system. Section 4 provides a quality control scheme of the FY-3C MWTS-2 radiance data. The assessments of MWTS-2 are also provided in this section. Section 5 introduces the bias correction, the setup of the assimilation experiments, and the results of the FY-3C MWTS-2 radiance assimilation experiments. A summary and discussion are presented in Sect. 6.

2 FY-3C MWTS-2 observations

Radiance data in level 1b format from the FY-3C MWTS-2 are employed for this study for the month of July 2014. Channel characteristics of MWTS-2 are displayed in Table 1, including the channel frequency, peak weighting function height, and radiometric temperature sensitivity (Noise Equivalent Differential Temperature [NEDT]). The NEDT is about 0.2-0.3 K for channels 1-7 and 0.5 K for channels 9-13. Overall, the observation errors of the mid-upper troposphere sounding channels are smaller than those of the other channels. There are 90 scene FOVs along each MWTS-2 scan line. The swath width is 2250 km, and the horizontal FOV resolution at nadir is 32 km.

Figure 1 displays weighting functions calculated from a standard U.S. atmospheric profile for all channels of MWTS-2. The absorption and emission of microwave radiation by atmospheric oxygen enables MWTS-2 to passively sound temperature through the atmosphere as a function of altitude. The MWTS-2 has 13 channels in the oxygen band at frequencies between 50.3 GHz and 57.3 GHz. It can provide atmosphere temperature information from the Earth's surface to 1 hPa above.

3 GRAPES 3D-Var system

GRAPES is the Chinese new global NWP system. The main components of GRAPES include: variational data assimilation (GRAPES-3DVar); full compressible nonhydrostatical model core with semi-implicit and semi-Lagrangian de-scretization scheme; modularized model physics pack-age; global and regional assimilation and prediction systems (chen et al., 2008).

GRAPES-3DVar (Xue and Chen, 2008; Xue et al., 2008) is the analysis system designed for operational application. The horizontal resolution of GRAPES 3D-Var system is $1^{\circ}\times1^{\circ}$. The model top is approximately 32 km, with 36 vertical layers. It conducts four data assimilation cycles (00, 06, 12, and 18 UTC) and processes six hourly observations, which are centered at 00, 06, 12, and 18 UTC. The basic idea of variational assimilation is to find the closest

Atmos. Meas. Tech. Discuss., doi:10.5194/amt-2015-361, 2016
Manuscript under review for journal Atmos. Meas. Tech.
Published: 21 January 2016

Atmospheric Measurement Techniques Discussions

solution to the difference between the effective observation and background field in the given periods under the meaning of the least square method by adjusting the first guess. The GRAPES-3DVar system analysis is conducted through the minimization of an objective function given by

$$J(x) = J^b + J^o = \frac{1}{2}(x - x^b)^T B^{-1}(x - x^b) + \frac{1}{2}(H(x) - y^o)^T R^{-1}(H(x) - y^o) \quad (1)$$

where x is a state vector that is composed of atmospheric and surface variables, x^b is a background estimate of the state vector that is provided by a 6-hour forecast, and y^o is a vector of all of the observations (Li and Liu, 2015). **H** is the observation operator that transforms the state vector x into observation space. **R** is the estimated error covariance of the observations. Currently, the observation errors are considered to be uncorrelated. **B** is the estimated error covariance of the background field. The background covariance matrix that was used in this study was estimated using the NMC method (Parrish and Derber, 1992; Wu et al., 2002), which assumes that the background error covariances are well approximated by averaged forecast differences between 24- and 12-h forecasts verifying at the same time.

GRAPES 3D-Var system adopts the incremental analysis method (Courtier et al., 1994). Arakawa C-grid in the horizontal and height-based terrain following coordinate are used in the system. The model variables include wind fields (u, v), dimensionless pressure (π), and specific humidity (q). To solve the problems that the inverse of the background error covariance matrix ($\mathbf{B^{-1}}$) is ill-conditioned and too large to be computed, the background term is preconditioned, which improves the convergence in the minimization process and avoids calculating $\mathbf{B^{-1}}$ directly. Empirical Orthogonal Function (EOF) decomposition is used to separate three-dimensional field into two-dimensional field. Spectral filter is used for global model as horizontal component of control variable transform. Optimization adopts the Limited Memory Broyden-Fletcher-Goldfarb-Shanno method (L-BFGS) (Navon and Legler, 1987). RTTOV 9.3 (Radiative Transfer for TOVS) has been used for the simulation of satellite radiance (Saunders et al., 1999). Currently, the GRAPES-3DVar system could directly assimilate radiosondes, Surface Synoptic Observations (SYNOPs), ship, Aircraft Report (Airep), Atmospheric Motion Vectors (AMVs), ATOVS, COSMIC RO data, etc.

Prior to this study, GRAPES 3D-Var was not able to assimilate FY-3C MWTS-2 radiance data. In 2014, the fast transmittance coefficients were generated by the National Satellite Meteorological Center of CMA. The coefficients were implemented in the RTTOV 9.3

Atmos. Meas. Tech. Discuss., doi:10.5194/amt-2015-361, 2016
Manuscript under review for journal Atmos. Meas. Tech.
Published: 21 January 2016

system to calculate the optical depths. This updated RTTOV 9.3 allowed us to assimilate the FY-3C MWTS-2 radiance data in the GRAPES system.

4 Quality control scheme

4.1 Channel selection

As Table 1 and Fig.1 illustrate, MWTS-2 channels 1-3 are sensitive to surface and cloud liquid water. Channel 4 mainly profiles lower-troposphere atmospheric temperature. It is also sensitive to the surface and clouds. These channels are not assimilated in this research because model simulations of brightness temperature are still inaccurate due to the uncertainty in the surface emissivity. Channels 9-13 are upper-troposphere or lower-stratosphere channels. The assimilation of these channels is sensitive to high-level model atmospheric temperature. However, the model top of GRAPES is approximately 3-4 hPa. The GRAPES system cannot provide an accurate temperature profile at levels higher than the model top, which are needed for the assimilation of channels 9-13. The use of incorrectly extrapolated atmospheric temperature profiles over the model top will ruin the data assimilation. Thus, MWTS-2 channels 9-13 are not assimilated. In all, MWTS-2 channels 5-8 are used in this research on the GRAPES system.

4.2 Evaluation of MWTS-2 data and the extraction of the striping noise

4.2.1 Global Simulations of Brightness Temperatures

The global observed brightness temperatures of MWTS-2 channels 5-8 are assessed. It is found that the striping feature is visible in the along-track direction for these channels (global figure omitted; the regional distribution is shown in Fig. 3a). To illustrate the striping noise more clearly, the observations are subtracted by the model simulations. The global difference between MWTS-2 observations and model simulations (O-B) are shown in Fig. 2.

In this research, the Community Radiative Transfer Model (CRTM 2.0) is used to produce the simulations of brightness temperatures (van Delst et al., 2011). CRTM is chosen here to make the O-B of MWTS-2 comparable to those of ATMS provided by Qin et al. (2013). The 6-hour forecasts of the vertical profiles of temperature, specific humidity and the surface pressure from the NCEP global forecast system (GFS) are used as input to CRTM. The forecast field have a horizontal resolution of $1^{\circ} \times 1^{\circ}$ and 26 vertical levels. The highest vertical level is

Atmos. Meas. Tech. Discuss., doi:10.5194/amt-2015-361, 2016
Manuscript under review for journal Atmos. Meas. Tech.
Published: 21 January 2016

approximately 10 hPa. Global simulations of brightness temperature are used as a "reference" or "truth" for examining the performance of the MWTS-2 instrument (Zou and Wang, Guan et al., 2011).

Figure 2 shows the global distribution of O-B from FY-3C MWTS-2 channels 5-8 during 0300-1500 UTC July 1, 2014. The striping phenomena are visible in the along-track direction for channels 5-8. The striping noise is more apparent for channel 8. The striping noises are embedded in the observations, but the root causes remain to be identified.

4.2.2 Extracting the striping noise from the MWTS-2 observations

The striping noise needs to be removed from the data without altering the weather signals before assimilating these data (Qin, et al, 2013). A technique is used to extract the striping noise from FY-3C microwave radiance observations. This method has been successfully used to derive the striping noise from the ATMS observations without changing weather signals (Qin, et al, 2013). It combines principal component analysis (PCA) with Ensemble Empirical Mode Decomposition (EEMD). The PCA algorithm is used here to characterize sensor noise in the Earth scene data (Tobin et al., 2009). The striping noise is assumed to be constant in the cross-track direction and is contained in the PC coefficients. The EEMD method is used to extract random noise in an along-track varying PC coefficient (Wu and Huang, 2009). It is applied to the PC coefficient to extract the first few high-frequency oscillatory components of different channels. By using this technique, the scan dependence in brightness temperature observations are characterized, and the weather signals can be separated from the striping noise when present. The technique combining PCA with EEMD is used to remove the striping noise embedded in MWTS-2 observed brightness temperature.

Figure 3 shows the distributions of observations, model simulated brightness temperature, O-B, detected striping noise from MWTS-2 channel 8 of the tropical portion of the descending swath from 0300 to 1500 UTC on 1 July 2014. The observed brightness temperature and O-B after removing the striping noise are also presented in Fig. 3e and Fig. 3f. It is seen from Fig. 3a and Fig. 3b that striping noise exists in the observations but not in the model simulations. Figure 3d shows that on each scan line, the striping noises are the same. After removing the noise shown in Fig. 3d, the channel 8 observed brightness temperature and O-B are displayed in Fig. 3e and Fig. 3f. Comparison of Fig. 3f with Fig. 3c shows that most of the striping noises are removed in the new O-B data.

Atmos. Meas. Tech. Discuss., doi:10.5194/amt-2015-361, 2016
Manuscript under review for journal Atmos. Meas. Tech.
Published: 21 January 2016

The global distribution of the striping noise from MWTS-2 channels 5-8 from 0300 to 1500 UTC on 1 July 2014 are shown in Fig. 4. The noise is mainly within the range of -0.7 K to 0.9 K for channels 5-7 and -1.4 K to 1.8 K for channel 8. The noise is higher in magnitude in channel 8 than in the other three channels.

Here, an initial comparsion of MWTS-2 noise with ATMS noise are conducted. Figures 5a and 5b display the bias and standard deviation of the striping noise from MWTS-2 and ATMS channels during 1-27 July 2014, respectively. The numbers from 1-4 indicate channels 5-8 for MWTS-2 and channels 7-10 for ATMS. The center frequency of ATMS channels 7-10 are very close to those of MWTS-2 channels 5-8. The standard deviation (STD) of the noise from MWTS-2 channels is slightly larger than that of ATMS correspongding channels. The average biases of the striping noise from MWTS-2 and ATMS are within $\pm$0.01 K. Figures 5c and 5d show the bias and standard deviation of O-B from MWTS-2 channels before and after removing the striping noise and ATMS channels after removing striping noise during 1-27 July 2014. After removing the striping noise, the STDs of O-B from MWTS-2 are decreased. The bias almost does not change. The O-B bias from MWTS-2 is larger than that from ATMS. The STD of MWTS-2 is also larger than that of ATMS, even after extracting the noise.

4.3 Cloud Detection

Given that the input profiles from the NWP models lack reliable information regarding clouds and because scattering processes cannot currently be accurately simulated in the fast radiative transfer models, the assimilation of cloud-contaminated observations will degrade the assimilation system. As a result, cloud detection should be conducted. For microwave temperature satellite measurements, the two weak water absorption channels (23.8 And 31.4 GHz) and the channel sounding of the scattering process (89 GHz) are often used for cloud detection (Weng and Grody, 1994; Grody et al., 2001; Klaes and Schraidt, 1999). However, FY-3C MWTS-2 does not have these channels. This situation makes it difficult to detect clouds and precipitation by itself. MWTS-1 onboard FY-3A/B also has this problem. To solve this difficulty, in 2013, a VIRR cloud detection method is proposed for FY-3A/B MWTS-1 (Li and Zou, 2013; Li and Liu, 2015). It can detect cloud contaminated FOVs efficiently. This method will also be used in this research.

Atmos. Meas. Tech. Discuss., doi:10.5194/amt-2015-361, 2016
Manuscript under review for journal Atmos. Meas. Tech.
Published: 21 January 2016

In this scheme, cloud detection for MWTS-2 is conducted using a cloud fraction product from the visible and infrared radiometer (VIRR) onboard the FY-3C satellite. The VIRR has 10 channels spanning the spectrum from 0.455 mm to 12.5 mm, and the horizontal resolution of the pixel at nadir is 1.1 km. Cloudy FOVs of VIRR are identified by a multi-threshold cloud detection method (Li and Zou, 2013). Based on these thresholds, a VIRR pixel is classified as a "cloudy" or "clear" FOV. Then a cloud fraction is calculated for an individual MWTS-2 FOV. This fraction is defined by the ratio of the total number of cloudy pixels to all of the VIRR pixels that are located in the MWTS-2 FOV. A threshold (f_{VIRR}) of 76% is demonstrated to be efficient to identify a cloudy scene (Li and Liu, 2015).

Figure 6 shows the distributions of the MWTS-2 clear pixels identified by cloud fractions of less than 76% over the ocean during the period from 0300UTC to 0900UTC on July 1, 2014. The local equator crossing time of NOAA-18 AMSU-A is close to FY-3C. Thus, the liquid water path (LWP) product of NOAA-18 AMSU-A is used here to verify the precision of the cloud detection scheme. The LWP products from the operational Microwave Surface and Precipitation Products System (MSPPS) are often used in the cloud detection of AMSU-A (Weng and Grody, 1994; Ferraro et al., 2005). The LWP is only retrieved over the ocean (without sea ice) and varies from 0.01 kg m^{-2} to 2 kg m^{-2}. An AMSU-A FOV with an LWP greater than a threshold (f_{LWP}) of 0.03 kg m^{-2} is marked as a cloudy scene in Li and Liu (2015).

FOVs with LWPs less than 0.03 kg m^{-2} (Li and Liu, 2015) are shown as grey dots (the FOVs at the scan edge of AMSU-A are in black). As illustrated in Fig. 6, the clear FOVs are almost all located in the grey dot region, corresponding to the clear region identified by an AMSU-A LWP of less than 0.03 kg m^{-2}. The red dots show the MWTS-2 data that pass the cloud detection but are removed by the next QC step bi-weighting QC (described in the next section). It is seen that these dots are distributed at the edge of the cloudy region identified by AMSU-A. This suggests that although some cloudy FOVs are not detected by the VIRR method, they will be removed in the next QC step (bi-weighting QC).

4.4 QC based on scan and surface characteristics

In addition to clouds, surface emissivity causes another type of challenge for satellite data assimilation. Surface emissivity varies with frequency and surface type. The global distribution of surface emissivity is not well known. Simulations of surface-sensitive channels

Atmos. Meas. Tech. Discuss., doi:10.5194/amt-2015-361, 2016
Manuscript under review for journal Atmos. Meas. Tech.
Published: 21 January 2016

Atmospheric Measurement Techniques Discussions

contain large errors, especially over land, snow, ice and coastal areas. The large uncertainty in the surface emissivity and the significant impact of surface emissivity on the radiance simulations also make the detection of cloud/precipitation considerably more difficult over land, snow, ice and coastal areas. Additional QC steps addressing problems associated with surface emissivity, high terrain and outliers are implemented for FY-3C MWTS-2 data.

Table 2 provides a QC scheme for the MWTS-2. When f_{VIRR} is greater than 76%, only data from channels 7-8 are used because the weighting function of this channel range is in the upper-troposphere where clouds have negligible effects. Channel 5 is used only over the ocean when no sea ice is present. The MWTS-2 channel 5 over land and channel 6 over high terrain (e.g., terrain height is greater than 500 m) are not used due to uncertainties in surface emissivity. The identification of an underlying land/sea/coast is based on a land mask database with a 0.25° longitudinal and latitudinal resolution. Sea ice is identified when sea surface temperature (SST) is less than 271.45 K using CMA daily SST data. The eight outermost FOVs (i.e., FOV 1-8, 83-90) for all channels are excluded for data assimilation due to larger inhomogeneity limb-effects that could not be accurately accounted for in forward radiative transfer models. The data were thinned into a 120 km box.

After the previous QC procedures, a bi-weighting quality control procedure is applied to identify outliers. The outliers are defined as those measurements with values that show differences from the model-simulated values by more than2 times the STD (Lansante, 1996; Zou and Zeng, 2006). Considering the variations of the mean states of the atmosphere at different latitudes, the bi-weighting quality control is implemented separately in three separate latitudinal bands: the tropics (30 ℃N-30 ℃S), middle latitudes (30 ℃N-60 ℃N, 30 ℃S-60 ℃S), and high latitudes (60 ℃N-90 ℃N, 60 ℃S-90 ℃S). More details are provided by Zou and Zeng (2006).

5 Assimilation results

5.1 Experimental setup

Initially, four different experiments are conducted from 1 to 27 July 2014. Control run 1 (CTRL1) assimilates only conventional observations. The conventional observations contain a global set of surface and upper-air reports, including radiosondes, SYNOP, ship, Airep, and AMVs from the Global Telecommunications System (GTS). Control run 2 (CTRL2) assimilates conventional observations, NOAA-15/18, AMSU-A, MetOp-A AMSU-A, and COSMIC RO observations. The setup for the experimental run (CONV1 and SAT1) is

Atmos. Meas. Tech. Discuss., doi:10.5194/amt-2015-361, 2016
Manuscript under review for journal Atmos. Meas. Tech.
Published: 21 January 2016

identical to the control run (CTRL1 and CTRL2) except that the FY-3C MWTS-2 radiance data are used after first removing the striping noise. Table 3 shows the experimental design for the four-cycle experiments.

The CTRL1, CONV1, CTRL2 and SAT1 experiments are conducted to reveal the impact of MWTS-2 on the global GRAPES system. In addition, CONV2 and SAT2 experiments are also conducted to demonstrate the impact of the extraction of striping noise on the GRAPES 3D-Var analysis.

5.2 Analysis/forecast cycle experiments

5.2.1 Data characteristics after QC and bias correction

The quality control scheme of MWTS-2 described in Sect. 3 is implemented in the four impact experiments (CONV1, CONV2, SAT1 and SAT2). The quality control procedures are the same for the four experiments. However, only SAT1 is implemented in the operational GRAPES assimilation system. The other three experiments are only for research purposes. Here, the quality control procedure of SAT1 are displayed in Fig. 7- Fig. 11.

Figure 7 shows scatter plots of the differences of brightness temperature between observations and model simulations for the outliers of MWTS-2 channels 5-8 during 1-5 July 2014. Only clear observations over the ocean are retained for channel 5. Some channel 6 radiance data over land with a low terrain altitude remain. These data can contribute to the NWP analysis and forecast over land. The bi-weighting quality control procedures remove some residual cloudy FOVs that have passed the cloud detection scheme. As indicated in Fig. 6, the observations that are removed by the bi-weighting check are typically located near cloudy FOVs. These outliers are probably associated with those observations that are affected by clouds and precipitation. These outliers cannot be simulated from the radiative transfer model because the input profiles from the NWP models lack reliable information in regard to clouds. The O-B differences of the outliers and their variations are much larger than those of the remaining data.

Figure 8 displays scatter plots of the differences of the brightness temperature between observations and model simulations for the data of MWTS-2 channels 5-8 that have passed quality control during 1-5 July 2014. The differences between the MWTS-2 observations and the model simulations for channel 5 are within the range of -3.8 K to -4.5 K (Fig. 8a). The

Atmos. Meas. Tech. Discuss., doi:10.5194/amt-2015-361, 2016
Manuscript under review for journal Atmos. Meas. Tech.
Published: 21 January 2016

variation range of channel 6 is from -1.8 K to -3 K. The observations minus simulations of channels 7-8 vary in the range from -3 K to -5 K. After the QC procedure, the biases vary within a smaller range for the four channels.

On average, approximately 17%, 25%, 60% and 60 % of the global observations remain for channels 5-8, respectively (Fig. 9a). More outliers are identified for channel 5 because it is a lower-level sounding channel and the observations are contaminated by clouds and the surface. The mean global biases and standard deviations of O-B are shown in Fig. 9b and Fig. 9c, both with and without removing the outliers. All of these channels have negative biases before and after QC. After QC, the bias and STD of all channels are all reduced. The remaining biases of channels 5-8 are approximately -4.2 K, -2.5 K, -4.6 K and -4.2 K, respectively. The STDs are approximately 0.2 K for these four channels. These biases will be removed by the subsequent bias-correction procedures.

Data assimilation schemes assume unbiased O-B. However, the bias between observed and first-guess radiance always exists due to the inaccuracies in RTTOV, the error in the calibration of the satellite instrument, and the error in the first-guess model profiles of temperature and humidity. To assimilate the MWTS-2 radiance data, bias correction is an essential step. The biases are calculated using an empiric bias-correction method provided by Harris and Kelly (Harris and Kelly, 2001). The biases are then subtracted from the MWTS-2 observations.

Figure 10 shows the average uncorrected scan bias and the corrected scan bias for MWTS-2 during July 1-27, 2014. After bias correction, the scan biases are almost removed. Figure 11 shows scatter plots of uncorrected and corrected O-B with latitude for MWTS-2 channels 5-8 during 1-5 July 2014. The biases of O-B are significantly reduced. The average biases after the bias correction are within ±0.1 K.

5.2.2 Analysis and forecast

The analysis fields of these experiments are first verified against those of the NCEP analysis. The impacts of MWTS-2 on the control experiment that assimilates only conventional data are shown in Fig. 12. This figure displays the root mean square (RMS) of the geopotential height and U wind from the analysis field difference between CTRL1 and NCEP, between CONV1 and NCEP, and between CONV2 and NCEP in the Northern Hemisphere, the Southern Hemisphere, the Tropics and East Asia during 1-27 July 2014. The figures indicate

Atmos. Meas. Tech. Discuss., doi:10.5194/amt-2015-361, 2016
Manuscript under review for journal Atmos. Meas. Tech.
Published: 21 January 2016

that the root mean squares of geopotential height and the wind field from the CONV1 and CONV2 analysis field are smaller than those of CTRL1. This suggests that if adding MWTS-2 observations in the assimilation system, the RMS of the analysis field will be reduced. As the weighting function peak height of MWTS-2 channels 5-8 are within the range of 411.1 hPa to 88.5 hPa, the maximum impact of the MWTS-2 radiance is observed in the mid-upper level field (lower than 400 hPa). With the assimilation of MWTS-2 radiance data, the RMS of geopotential height in the upper level is significantly decreased. Comparison between CONV1 and CONV2 shows that after removing striping noise, the RMS of the analysis field is slightly reduced, especially in the upper level. This suggests that the quality control technique of removing striping noise can slightly decrease the analysis error. The results of the impact on the bias of geopotential height and U wind are similar to those on root mean square (figure omitted).

The impacts of MWTS-2 radiance on the GRAPES system when assimilating both conventional data and satellite data are also assessed. Figure 13 is similar to Fig. 12, but for CONV2, SAT1 and SAT2. Overall, the impact is neutral, with the three lines almost overlapping in all regions. The results of the impact on the temperature field are similar to those on the geopotential height and wind fields.

Finally, the forecasts are verified against their own analyses. An overall measurement of the quality of medium-range forecasts for predicting a large-scale weather system is widely given by the anomaly correlation coefficient (ACC) of a 500-hPa-height forecast field. A key performance indicator for the forecast system is the forecast range at which the ACC decreases to 60%. Seven-day forecasts were produced for each day of the 27-day period in this study. Figure 14 and 15 show Mean ACC and RMS of 500 hPa geopotential height of CTRL1, CONV1 and CONV2 experiments in the Northern and Southern Hemispheres for the period from 1 to 27 July 2014. Figure 14 also shows the results of the significance test. The difference between CONV1 and CTRL1 (CONV1-CTRL1), CONV2 and CTRL1 (CONV2-CTRL1) are analyzed. The acc and rms differences outside of outline bars are significante at the 95% confidence level. These figures shows that most results have passed the confidence test of 95% confidence level. In the Northern and Southern Hemispheres, the average ACC of CONV1 is higher than the control experiment CTRL1, and the RMS of CONV1 is lower than that of CTRL1. The MWTS-2 observations show positive impact only when conventional data are assimilated in the GRAPES system. The lines of CONV2 are almost overlapped on

Atmos. Meas. Tech. Discuss., doi:10.5194/amt-2015-361, 2016
Manuscript under review for journal Atmos. Meas. Tech.
Published: 21 January 2016

CONV1 in the Northern Hemisphere. In the Southern Hemisphere, the RMS of 500 hPa geopotential height of CONV1 is slightly smaller than that of CONV2. The forecast error is slightly decreased. It suggests that the quality control scheme of extracting striping noise may contribute to the analysis and forecast. This impact will be further explored.

Figure 15 is similar to Fig. 14 but for the experiments of CTRL2, SAT1 and SAT2. The experimental results of SAT1 are almost equal to those of SAT2, with the lines almost overlapping in both hemispheres. Thus, the significance test results are not shown. Upon comparing SAT1 and SAT2 with CTRL2, it is found that the impact of MWTS-2 on the assimilation system when conventional data and other satellite data are used is negligible.

Overall, adding MWTS-2 observations in an assimilation system that assimilates only conventional data can slightly improve the analysis and forecast. The quality control scheme of extracting striping noise may contribute to the analysis and forecast. The MWTS-2 impact on the assimilation system that assimilates all data is neutral.

6 Summary and discussion

In this research, the assimilation of the FY-3C MWTS-2 radiance data in the Chinese NWP system-Global GRAPES system is conducted. A quality control procedure for FY-3C MWTS-2 is proposed and applied in the GRAPES system. Through the initial assessment of MWTS-2 observations, an apparent striping pattern is found in the observed brightness temperature. A technique combining PCA and EEMD is used to extract the striping noise. After the method is applied to the observations, most of the striping noise is removed. A quality control scheme is introduced based on the characteristics of the FY-3C MWTS-2 observations. A cloud-detection algorithm with a threshold of 76% is incorporated based on the cloud fraction product that is provided by the VIRR onboard FY-3C. Other QC steps are based on the underlying surface characteristics and the differences between model simulations and observations. The bi-weighting QC can remove some residual cloudy FOVs that have passed the cloud-detection scheme. Approximately 83%, 75%, 40% and 40% of the MWTS-2 observations are removed by the proposed QC for channels 5-8, respectively. After QC, the standard deviation of O-B decreased significantly. The remaining biases of channels 5-8 are approximately -4.2 K, -2.5 K, -4.6 K and -4.2 K, respectively. The STDs are approximately 0.2 K for these four channels. These biases are removed by the subsequent bias-correction procedures.

The impacts of the MWTS-2 radiance data on the prediction of GRAPES are studied. Impact

analysis shows that the direct assimilation of MWTS-2 observations can decrease analysis error when the control experiment uses only conventional data. After removing striping noise, the analysis error is smaller than the experiments assimilating data without extracting noise; i.e., the quality control technique of removing striping noise can slightly decrease the analysis error. The impact of MWTS-2 radiance data on the GRAPES system when assimilating all data are is neutral.

Analysis/forecast cycle experiments were conducted for nearly a month. When the control experiment assimilates only conventional data, the impact of MWTS-2 radiance is positive. Verifications indicate that the ACC of the 500-hPa-height forecast field slightly increased and that the RMS slightly decreased in the Northern Hemisphere. If all observations are used in the control experiment, the impact on MWTS-2 is neutral. After removing striping noise, the forecast error is smaller than the experiments assimilating data without extracting noise. Overall, the assimilation of the MWTS-2 data could have a neutral to small positive impact on the assimilation and model forecast. The quality control scheme of extracting striping noise may contribute to the analysis and forecast.

This study demonstrates the impact of the FY-3C MWTS-2 observations on an NWP system and the application of a QC scheme. The assimilation of the MicroWave Humidity Sounder -2 (MWHS-2) will be further explored. In addition, the Chinese FY-3D satellite will be launched in 2016. It carries the same instruments as those on FY-3C. The quality control scheme and impact study on FY-3C MWTS-2 and MWHS-2 will contribute to future research of FY-3D microwave sounding data.

Acknowledgements

The authors thank their colleagues for continuing support and discussion around the coffee breaks. This work was jointly supported by the China Special Fund for Meteorological Research in the Public Interest (No. GYHY201406008), Project supported by the National Natural Science Foundation of China (Grant Nos. 91337218 and 41475103).

References

Andersson, E., Pailleux, J., Thepaut, J. N., Eyre, J. R., McNally, A. P., Kelly, G. A., and Courtier, P.: Use of cloud-cleared radiances in three-four-dimensional variational data assimilation, Q. J. R. Meteorol. Soc., 120(517), 627-653, doi:10.1002/qj.49712051707, 1994.

Baker, N. L. and Daley, R.: Observation and background adjoint sensitivity in the adaptive observation-targeting problem, Q. J. R. Meteorol. Soc., 126(565), 1431-1454, doi:10.1002/qj.49712656511, 2000.

Cardinali, C.: Monitoring observation impact on short-range forecast, Q. J. R. Meteorol. Soc., 135(638), 239-250, doi:10.1002/qj.366, 2009.

Chen, D. H., Xue, J. S., Yang, X. S., Zhang, H. L., Shen, X. S., Hu, J. L., Wang, Y., Ji, L. R., and Chen, J. B.: New generation of multi-scale NWP system (GRAPES): general scientific design, Chin. Sci. Bull., 53(22), 3433-3445, doi:10.1007/s11434-008-0494-z, 2008.

Coutier, P., Andersson, E., Heckley, W., Vasiljevic, D., Hamrud, M., Hollingsworth, A., Rabier, F., Fisher, M., and Pailleux, J.: The ECMWF implementation of three-dimensional variational assimilation (3D-Var). I: formulation, Q. J. R. Meteorol. Soc., 124, 1783-1807, 1998.

Derber, J. C. and Wu, W. S.: The use of TOVS cloud-cleared radiances in the NCEP SSI analysis system, Mon. Weather. Rev., 126(8), 2287-2299, doi:10.1175/1520-0493(1998)126<2287:TUOTCC>2.0.CO;2, 1998.

Dong, C. H., Yang, J., Yang, Z. D., Lu, N. M., Shi, J. M., Zhang, P., Liu, Y. J., Cai, B., and Zhang, W.: An overview of a new Chinese weather satellite FY-3A, Bull. Am. Meteorol. Soc., 90(10), 1531-1544, doi:10.1175/2009BAMS2798.1, 2009.

Ferraro, R. R., Weng, F. Z., Grody, N. C., Zhao, L. M., Meng, H., Kongoli, C., Pellegrino, P., Qiu, S., and Dean, C.: NOAA operational hydrological products derived from the advanced microwave sounding unit, IEEE Trans. Geosci. Rem. Sens., 43(5), 1036-1049, doi:10.1109/TGRS.2004.843249, 2005.

Fourrié, N., Doerenbecher, A., Bergot, T., and Joly, A.: Adjoint sensitivity of the forecast to TOVS observations, Q. J. R. Meteorol. Soc., 128(586), 2759-2777, doi:10.1256/qj.01.167, 2002.

Gelaro, R., Langland, R. H., Pellerin, S., and Todling, R.: The THORPEX observation impact intercomparison experiment, Mon. Weather. Rev., 138(11), 4009-4025, doi:10.1175/2010MWR3393.1, 2010.

Grody, N., Zhao, J., Ferraro, R., Weng, F., and Boers, R.: Determination of precipitable water and cloud liquid water over oceans from the NOAA 15 advanced microwave sounding unit, J. Geophys. Res., 106(D3), 2943-2953, 2001.

Guan, L., Zou, X., Weng, F., and Li, G.: Assessments of FY-3A Microwave Humidity Sounder measurements using NOAA-18 Microwave Humidity Sounder, J. Geophys. Res., 116, D10106, doi:10.1029/2010JD015412, 2011.

Harris, B. A. and Kelly, G.: A satellite radiance-bias correction scheme for data assimilation, Q. J. R. Meteorol. Soc., 127(574), 1453-1468, doi:10.1002/qj.49712757418, 2001.

Klaes, D. and Schraidt, R.: The European ATOVS and AVHRR processing package (AAPP), Tech. Proc.10th Int. ATOVS Study Conf., Boulder, USA, 1999.

Kozo OKAMOTO, Masahiro KAZUMORI, and Hiromi OWADA: The assimilation of ATOVS radiances in the JMA global analysis system, J. Meteor. Soc. Japan, 83(2), 201-217, 2005

Langland, R. H. and Baker, A. L.: Estimation of observation impact using the NRL atmospheric variational data assimilation adjoint system, Tellus A, 56(3), 189-201, doi:10.1111/j.1600-0870.2004.00056.x, 2004.

Lansante, J. R.: Resistant, robust and non-parametric techniques for the analysis of climate data: theory and examples, including applications to historical radiosonde station data, Int. J. Climatol., 16(11), 1197-1226, doi:10.1002/(SICI)1097-0088(199611)16:11<1197::AID-JOC89>3.0.CO;2-L, 1996.

Li, J. and Liu, G.: Assimilation of Chinese FengYun 3B Microwave Temperature Sounder radiances into Global GRAPES system with an improved cloud detection threshold, doi: 10.1007/s11707-015-0499-2, 2015.

Li, J. and Zou, X.: A quality control procedure for FY-3A MWTS measurements with emphasis on cloud detection using VIRR cloud fraction, J. Atmos. Ocean. Technol., 30(8), 1704-1715, doi:10.1175/JTECH-D-12-00164.1, 2013.

Li, J. and Zou, X.: Impact of FY-3A MWTS radiances on prediction in GRAPES with comparison of two quality control schemes, Front. Earth. Sci., 8(2), 251-263, doi:10.1007/s11707-014-0405-3, 2014.

Lu, Q. and Bell, W.: Evaluation of FY-3B data and an assessment of passband shifts in AMSU-A and MSU during the period 1978-2012, Interim report of Visiting Scientist mission NWP_11_05, Document NWPSAF-EC-VS-023, Version 0.1, 28, 2012.

Lu, Q., Bell, W., Bauer, P., Bormann, N., and Peubey, C.: An initial evaluation of FY-3A satellite data, ECMWF Technical Memoranda Number 631, ECMWF, Shinfield Park, Reading, UK, 58, 2010.

Lu, Q., Lawrence, H., Bormann, N., English, S., Lean, K., Atkinson, N., Bell, W., and Carminati, F. : An evaluation of FY-3C satellite data quality at ECMWF and the Met Office, ECMWF Technical Memoranda Number 767, ECMWF, Shinfield Park, Reading, UK, 2015.

McNally, A. P., Derber, J. C., Wu, W., and Katz, B. B.: The use of TOVS level-1b radiances in the NCEP SSI analysis system, Q. J. R. Meteorol. Soc., 126(563), 689-724, doi:10.1002/qj.49712656315, 2000.

Navon, I. M. and Legler, D. M.: Conjugate gradient methods for large scale minimization in meteorology, Mon. Weather. Rev., 115(8), 1479-1502, doi:10.1175/1520-0493(1987)115<1479:CGMFLS>2.0.CO;2, 1987.

Parrish, D. F. and Derber, J. C.: The National Meteorological Centers spectral statistical in nterpolation analysis system, Mon. Weather. Rev., 120(8), 1747-1763, 1992.

Qin, Z., Zou, X., and Weng, F.: Analysis of ATMS striping noise from its Earth scene observations, J. Geophys. Res. Atmos., 118, 13214-13229, doi:10.1002/2013JD020399, 2013.

Saunders, R. W., Matricardi, M., and Brunel, P.: An Improved Fast Radiative Transfer Model for Assimilation of Satellite Radiance Observations, Q. J. R. Meteorol. Soc., 125, 1407-1425, 1999.

Tobin, D. C., Revercomb, H. E., and Antonelli, P.: Principal component analysis of IASI spectra with a focus on non-uniform scene effects on the ILS, in Proc. AIP Conf, 1100, 16, AIP Publishing, Foz do Iguaçu Brazil, 2009.

Van, Delst P.: CRTM: v2.0 User Guide, Joint Center for Satellite Data Assimilation, Camp Springs, Maryland, USA, 2011.

Weng, F. and Grody, N. C.: Retrieval of cloud liquid water using the special sensor microwave imager (SSM/I), J. Geophys. Res., 99(D12), 25535-25551, doi:10.1029/94JD02304, 1994.

Wu, W. S., Purser, R. J. and Parrish, D. F.: Three-dimensional variational analysis with spatially inhomogeneous covariances, Mon. Weather. Rev., 130(12), 2905-2916, 2002.

Wu, Z. and Huang, N. E.: Ensemble empirical mode decomposition: A noise-assisted data analysis method, Adv. Adapt. Data Anal., 1(1), 1-41, 2009.

Xue, J. S. and Chen, D. H.: Numerical Prediction System Design and Application of Science GRAPES. Science Press, Beijing, 2008 (in Chinese).

Xue, J. S., Zhuang, S. Y., Zhu, G. F., Zhang, H., Liu, Z. Q., Liu, Y., and Zhuang, Z. R.: Scientific design and preliminary results of three-dimensional variational data assimilation system of GRAPES, Chin. Sci. Bull., 53(22), 3446-3457, doi:10.1007/s11434-008-0416-0, 2008.

Zhang, P., Yang, J., Dong, C. H., Lu, N. M., Yang, Z. D., and Shi, J. M.: General introduction on payloads, ground segment and data application of Fengyun 3A, Front. Earth. Sci., 3(3), 367-373, doi:10.1007/s11707-009-0036-2, 2009.

Zou, X. and Weng, F.: Impacts of assimilation of ATMS data in HWRF on track and intensity forecasts of 2012 four landfall hurricanes, J. Geophys. Res., 118(20), 11558-11576, 2013.

Zou, X. and Zeng, Z.: A quality control procedure for GPS radio occultation data, J. Geophys. Res., 111(D2), D02112, doi:10.1029/2005JD005846, 2006.

Zou, X., Wang, X., Weng, F., and Guan, L.: Assessments of Chinese FengYun Microwave Temperature Sounder (MWTS) measurements for weather and climate applications, J. Atmos. Ocean. Technol., 28, 1206-1227, 2011.

Atmos. Meas. Tech. Discuss., doi:10.5194/amt-2015-361, 2016
Manuscript under review for journal Atmos. Meas. Tech.
Published: 21 January 2016

Atmospheric Measurement Techniques Discussions

Table 1. Channel characteristics of FY-3C MWTS-2.

Channel Number	Center Frequency (GHz)	Weighting function peak height (hPa)	NE△T (K)
1	50.3	surface	0.26
2	51.76	surface	0.20
3	52.8	surface	0.21
4	53.596	701.2	0.18
5	54.40	411.1	0.19
6	54.94	308	0.19
7	55.50	194	0.23
8	57.290344(f_0)	88.5	0.74
9	$f_0 \pm 0.217$	55.3	0.66
10	$f_0 \pm 0.3222 \pm 0.048$	25.49	0.49
11	$f_0 \pm 0.3222 \pm 0.022$	11.97	0.53
12	$f_0 \pm 0.3222 \pm 0.010$	5.75	0.93
13	$f_0 \pm 0.3222 \pm 0.0045$	2.87	2.11

Atmos. Meas. Tech. Discuss., doi:10.5194/amt-2015-361, 2016
Manuscript under review for journal Atmos. Meas. Tech.
Published: 21 January 2016

Atmospheric Measurement Techniques Discussions

1 Table 2. Channel selection based on cloud fraction, terrain height (z), and surface types.

Variables	Channel 5	Channel 6	Channel 7	Channel 8
f_{VIRR}>76%			√	√
Land (z>500 m)			√	√
Land ($z \leq 500$ m)		√	√	√
Ocean (SST>271.45 K)	√	√	√	√
Ocean (SST$\leq$271.45K)		√	√	√

2

3

Atmos. Meas. Tech. Discuss., doi:10.5194/amt-2015-361, 2016
Manuscript under review for journal Atmos. Meas. Tech.
Published: 21 January 2016

Atmospheric Measurement Techniques Discussions

Table 3. Experiment design for the six cycle experiments.

EXP	Observation Data
CTRL1	Conventional data
CONV1	Conventional data+FY-3C MWTS-2 (after removing striping noise)
CONV2	Conventional data+FY-3C MWTS-2 (before removing striping noise)

EXP	Observation Data
CTRL2	Conventional data+NOAA-15/18 AMSU-A+MetOp-A AMSU-A+COSMIC RO
SAT1	Conventional data+NOAA-15/18 AMSU-A+MetOp-A AMSU-A+COSMIC RO +FY-3C MWTS-2 (after removing striping noise)
SAT2	Conventional data+NOAA-15/18 AMSU-A+MetOp-A AMSU-A+COSMIC RO +FY-3C MWTS-2 (before removing striping noise)

Notes: Conventional data consists of radiosondes, SYNOP, ship, Airep, AMVs

Atmos. Meas. Tech. Discuss., doi:10.5194/amt-2015-361, 2016
Manuscript under review for journal Atmos. Meas. Tech.
Published: 21 January 2016

Atmospheric Measurement Techniques Discussions

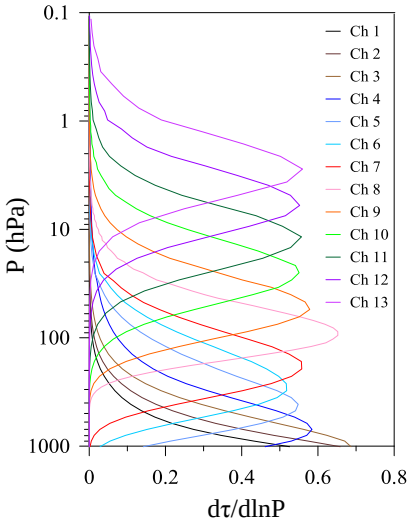

Figure 1. Weighting Functions of FY-3C MWTS-2 calculated using U.S. standard atmosphere profile.

Atmos. Meas. Tech. Discuss., doi:10.5194/amt-2015-361, 2016
Manuscript under review for journal Atmos. Meas. Tech.
Published: 21 January 2016

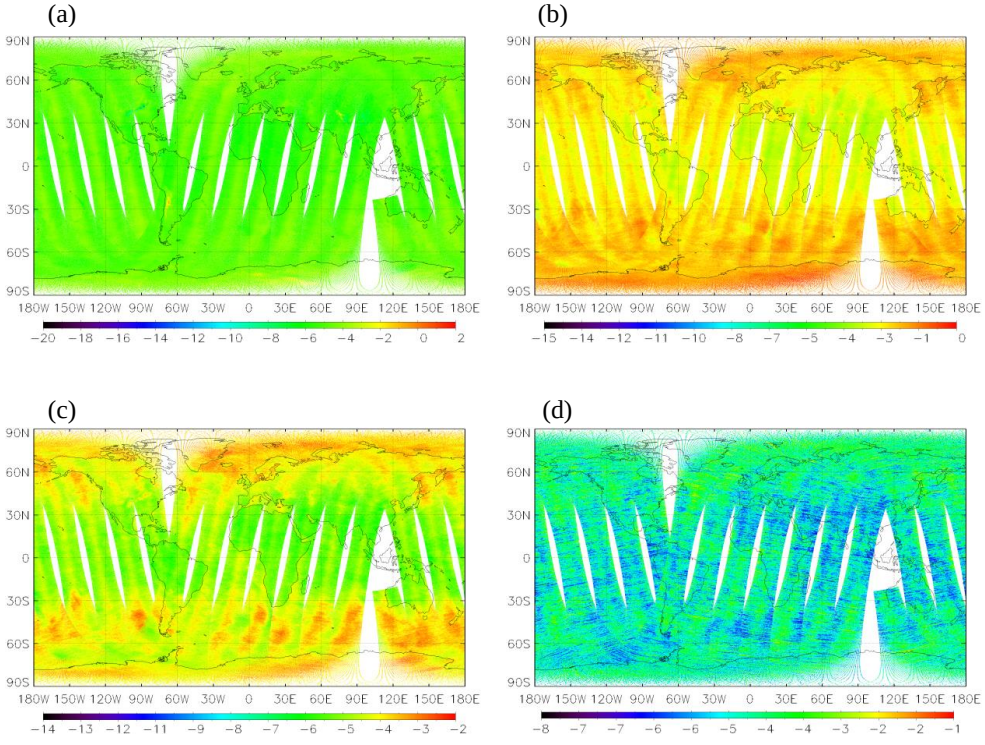

Figure 2. Global distribution of O-B from FY-3C MWTS-2 (a) channel 5, (b) channel 6, (c) channel 7 and (d) channel 8 during 0300-1500 UTC 1 July 2014.

Atmos. Meas. Tech. Discuss., doi:10.5194/amt-2015-361, 2016
Manuscript under review for journal Atmos. Meas. Tech.
Published: 21 January 2016

Atmospheric Measurement Techniques Discussions

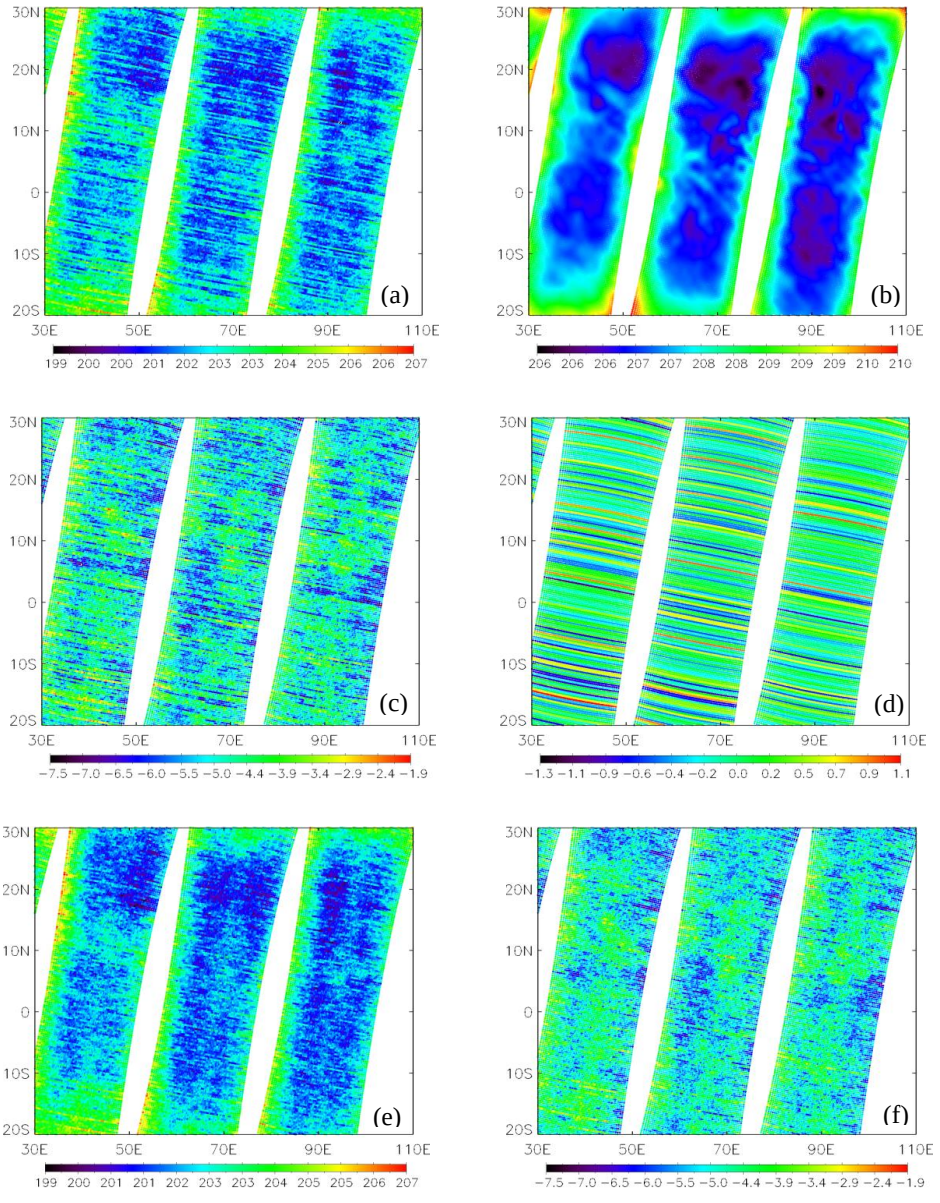

Figure 3. Distribution of (a) observed and (b) model simulated brightness temperature, (c) O-B, (d) striping noise, (e) observed brightness temperature and (f) O-B after removing the striping noise from FY-3C MWTS-2 channel 8 during 0300-1500 UTC 1 July 2014.

Atmos. Meas. Tech. Discuss., doi:10.5194/amt-2015-361, 2016
Manuscript under review for journal Atmos. Meas. Tech.
Published: 21 January 2016

Atmospheric Measurement Techniques Discussions

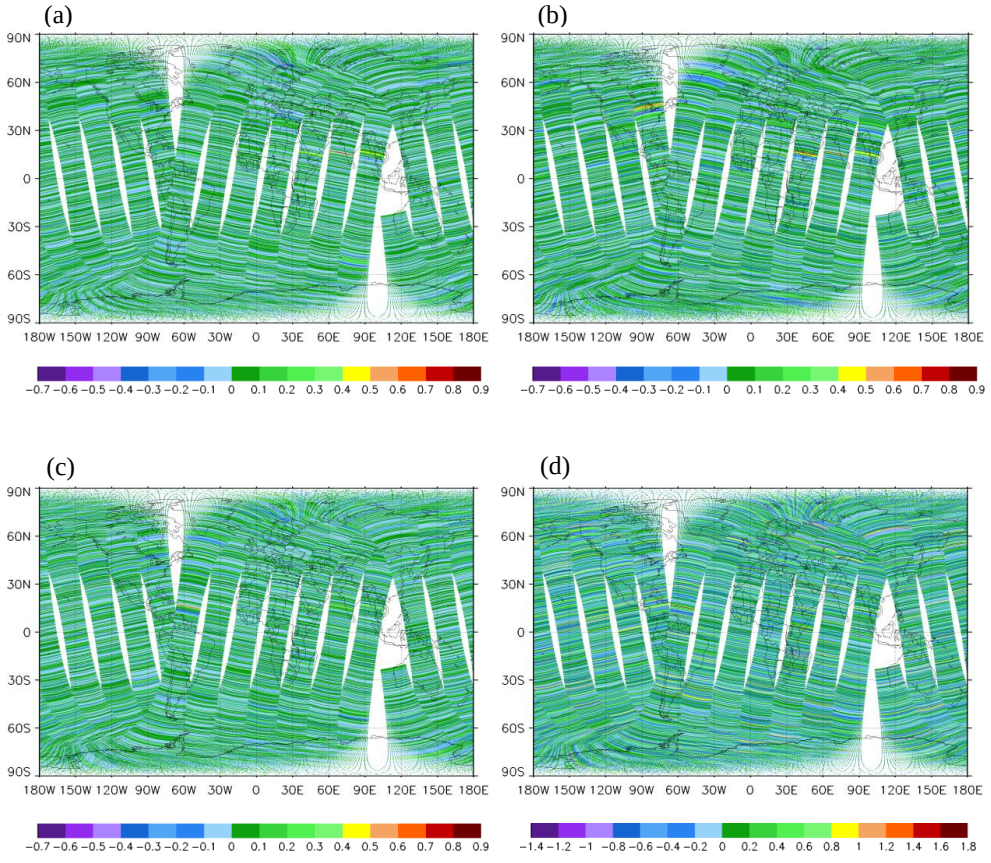

Figure 4. Global distribution of striping noise from FY-3C MWTS-2 (a) channel 5, (b) channel 6, (c) channel 7 and (d) channel 8 during 0300-1500 UTC 1 July 2014.

Atmos. Meas. Tech. Discuss., doi:10.5194/amt-2015-361, 2016
Manuscript under review for journal Atmos. Meas. Tech.
Published: 21 January 2016

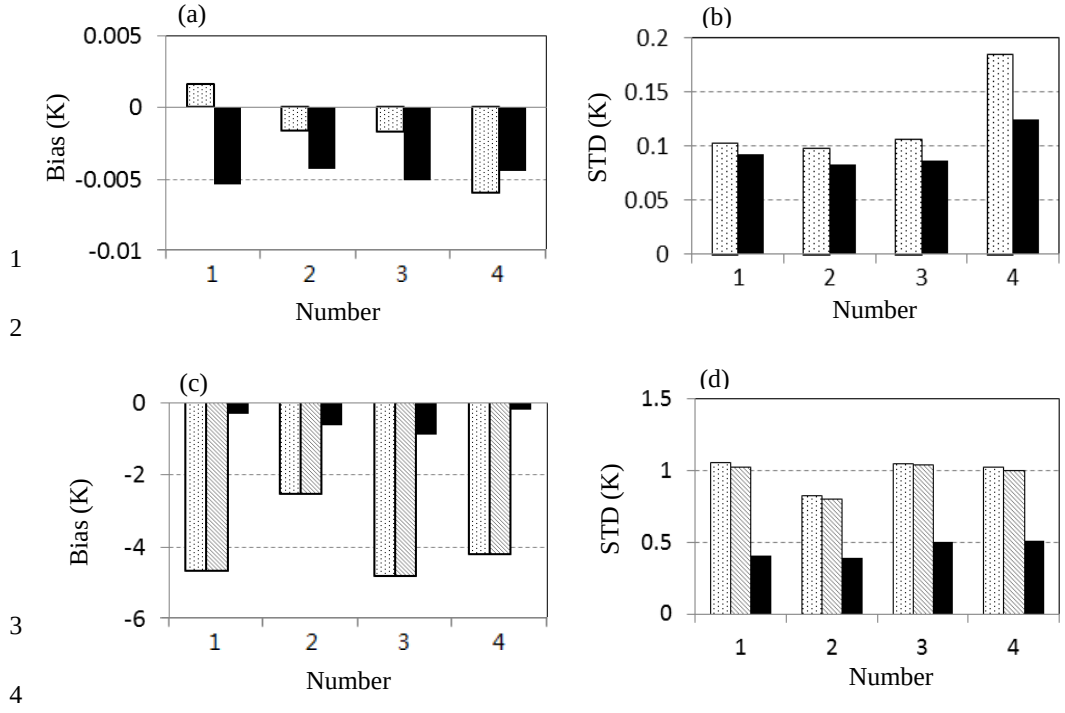

Figure 5. (a) Bias and (b) standard deviation of the striping noise from MWTS-2 channels (dotted bars) and ATMS channels (solid bars) during 1-27 July 2014. The numbers from 1-4 indicate channels 5-8 for MWTS-2 and channels 7-10 for ATMS. (c) Bias and (d) standard deviation of brightness temperature differences between observations and model simulations from MWTS-2 channels before (dotted bars), after (dashed bars) removing the striping noise and ATMS channels (solid bars) after removing striping noise during 1-27 July 2014.

Atmos. Meas. Tech. Discuss., doi:10.5194/amt-2015-361, 2016
Manuscript under review for journal Atmos. Meas. Tech.
Published: 21 January 2016

Atmospheric Measurement Techniques Discussions

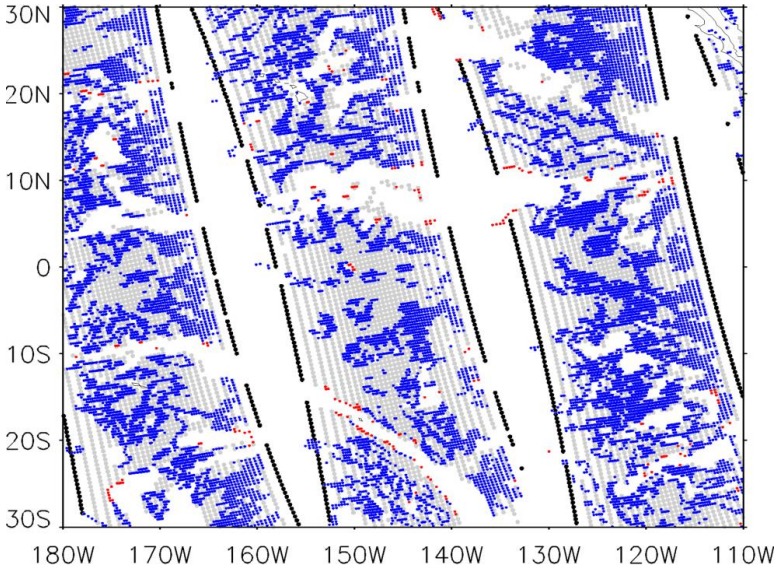

Figure 6. Distribution of the MWTS-2 clear pixels identified by cloud fraction less than 76% (blue dots) over ocean during the period from 0300UTC to 0900UTC on July 1, 2014. NOAA-18 AMSU-A FOVs with LWP less than 0.03 kg m^{-2} are shown in grey dots (the FOVs at the scan edge of AMSU-A are in black). The FOVs detected by biweighting QC is shown in red.

Atmos. Meas. Tech. Discuss., doi:10.5194/amt-2015-361, 2016
Manuscript under review for journal Atmos. Meas. Tech.
Published: 21 January 2016

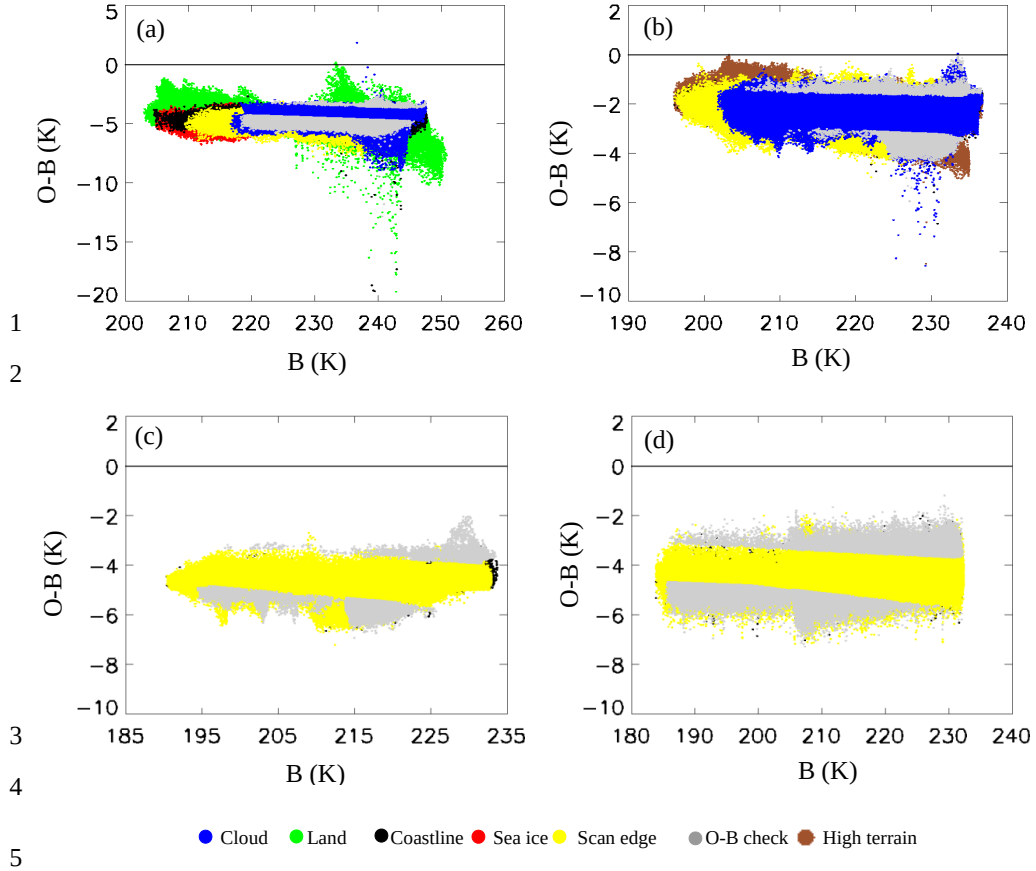

Figure 7. Scatter plots of the differences of brightness temperature between observations and model simulations for MWTS-2 (a) channel 5, (b) channel 6, (c) channel 7 and (d) channel 8 outliers during 1-5 July 2011.

Atmos. Meas. Tech. Discuss., doi:10.5194/amt-2015-361, 2016
Manuscript under review for journal Atmos. Meas. Tech.
Published: 21 January 2016

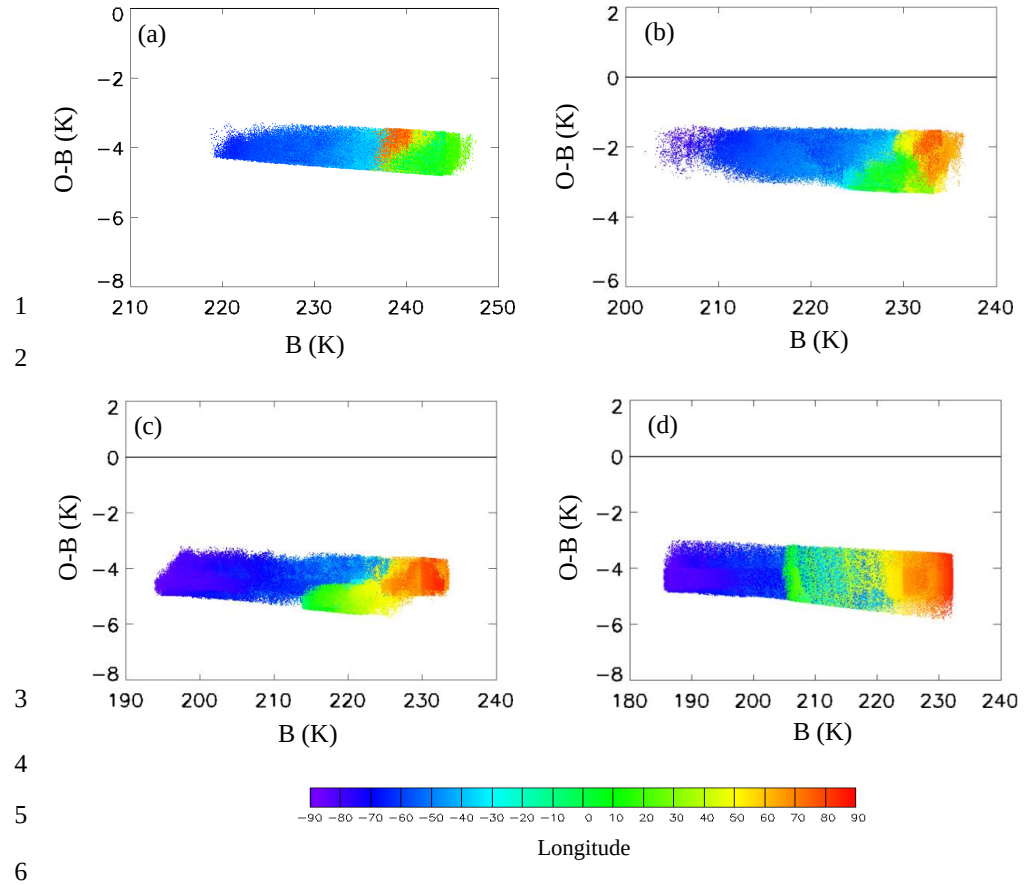

Figure 8. Scatter plots of the differences of the brightness temperature between observations and model simulations for the data of MWTS-2 (a) channel 5, (b) channel 6, (c) channel 7 and (8) channel 8 that have passed quality control during 1-5 July 2014.

Atmos. Meas. Tech. Discuss., doi:10.5194/amt-2015-361, 2016
Manuscript under review for journal Atmos. Meas. Tech.
Published: 21 January 2016

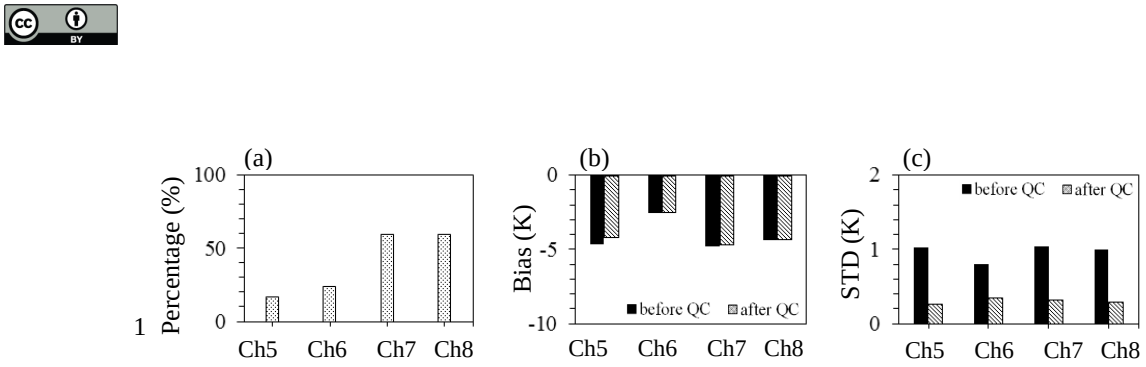

Figure 9. (a) Percentages of the MWTS-2 data that passed QC during 1-27 July 2014. (b) Global biases and (c) standard deviations of O-B before (solid bars) and after (dashed bars) quality control during 1-27 July 2014.

Atmos. Meas. Tech. Discuss., doi:10.5194/amt-2015-361, 2016
Manuscript under review for journal Atmos. Meas. Tech.
Published: 21 January 2016

Atmospheric Measurement Techniques Discussions

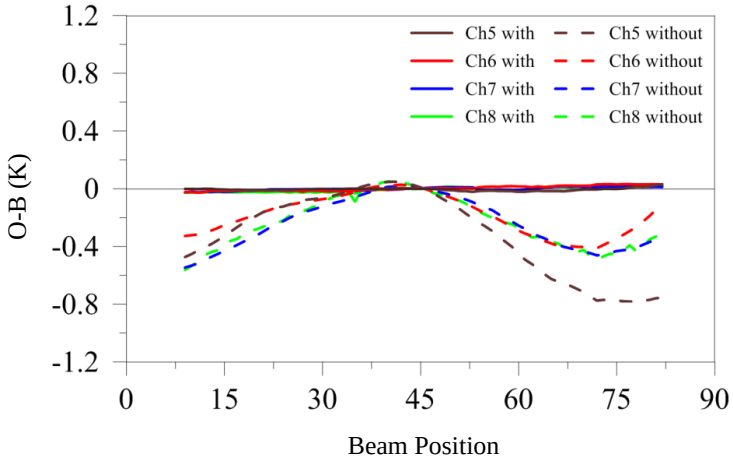

Figure 10. Averaged scan bias with (solid lines) and without (dashed lines) bias correction for MWTS-2 during 1-27 July 2014.

Atmos. Meas. Tech. Discuss., doi:10.5194/amt-2015-361, 2016
Manuscript under review for journal Atmos. Meas. Tech.
Published: 21 January 2016

Atmospheric Measurement Techniques Discussions

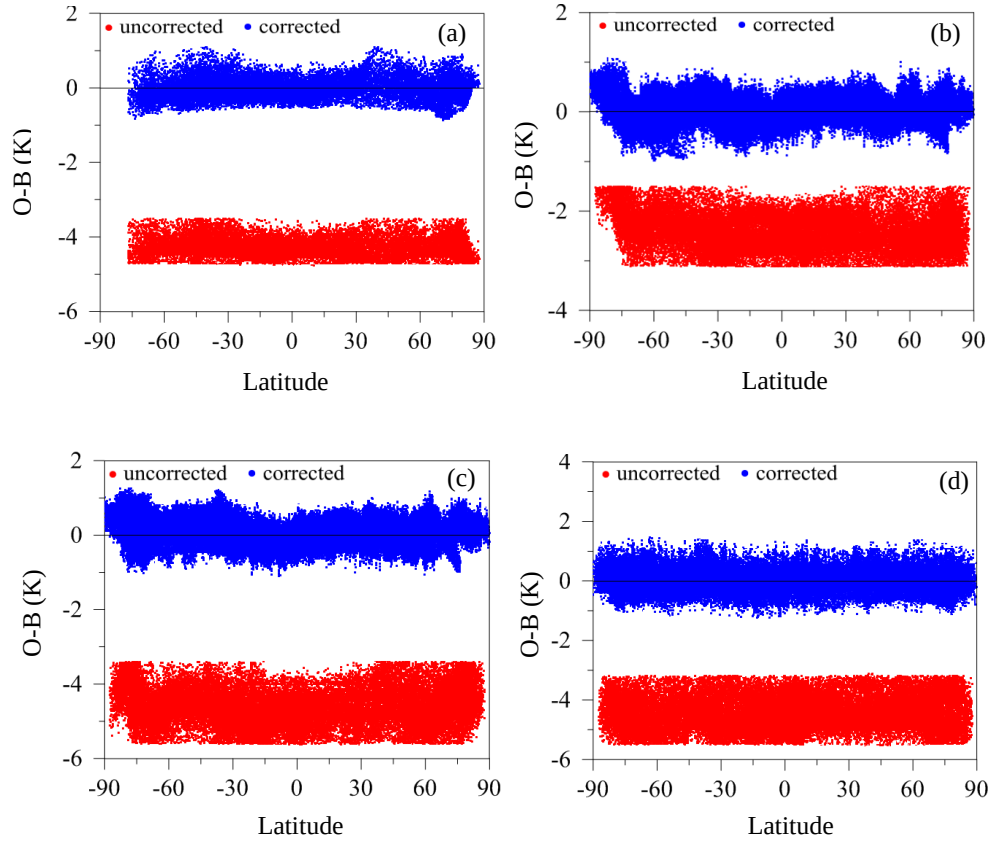

Figure 11. Scatter plots of uncorrected (red) and corrected (blue) O-B with latitude for MWTS-2 (a) channel 5, (b) channel 6, (c) channel 7 and (d) channel 8 during 1-5 July 2014.

Atmos. Meas. Tech. Discuss., doi:10.5194/amt-2015-361, 2016
Manuscript under review for journal Atmos. Meas. Tech.
Published: 21 January 2016

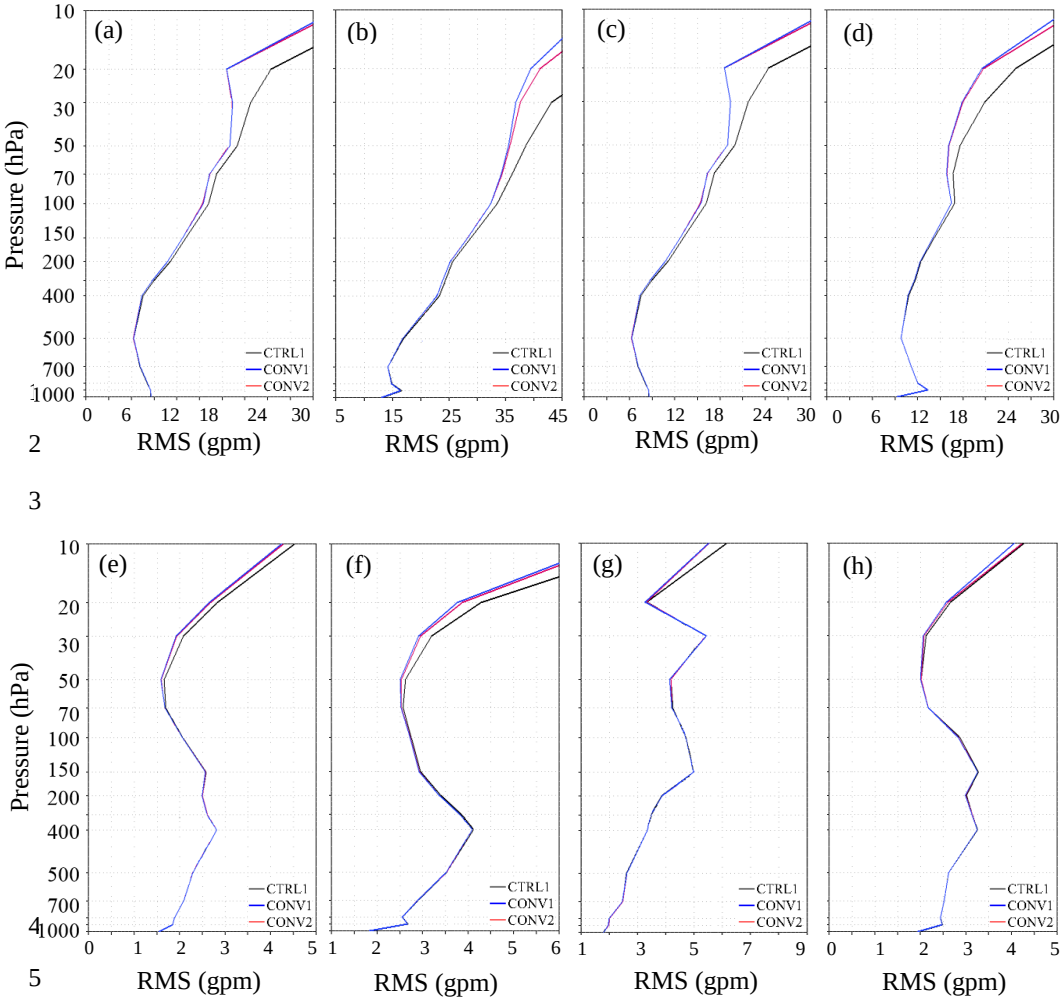

Figure 12. RMS of geopotential height from the analysis field difference between CTRL1 and NCEP (black), CONV1 and NCEP (blue), CONV2 and NCEP (red) in the (a) Northern Hemisphere, (b) Southern Hemisphere, (c) Tropic and (d) East Asia during 1-27 July 2014. (e)-(h) are similar to (a)-(d) but for U wind.

Atmos. Meas. Tech. Discuss., doi:10.5194/amt-2015-361, 2016
Manuscript under review for journal Atmos. Meas. Tech.
Published: 21 January 2016

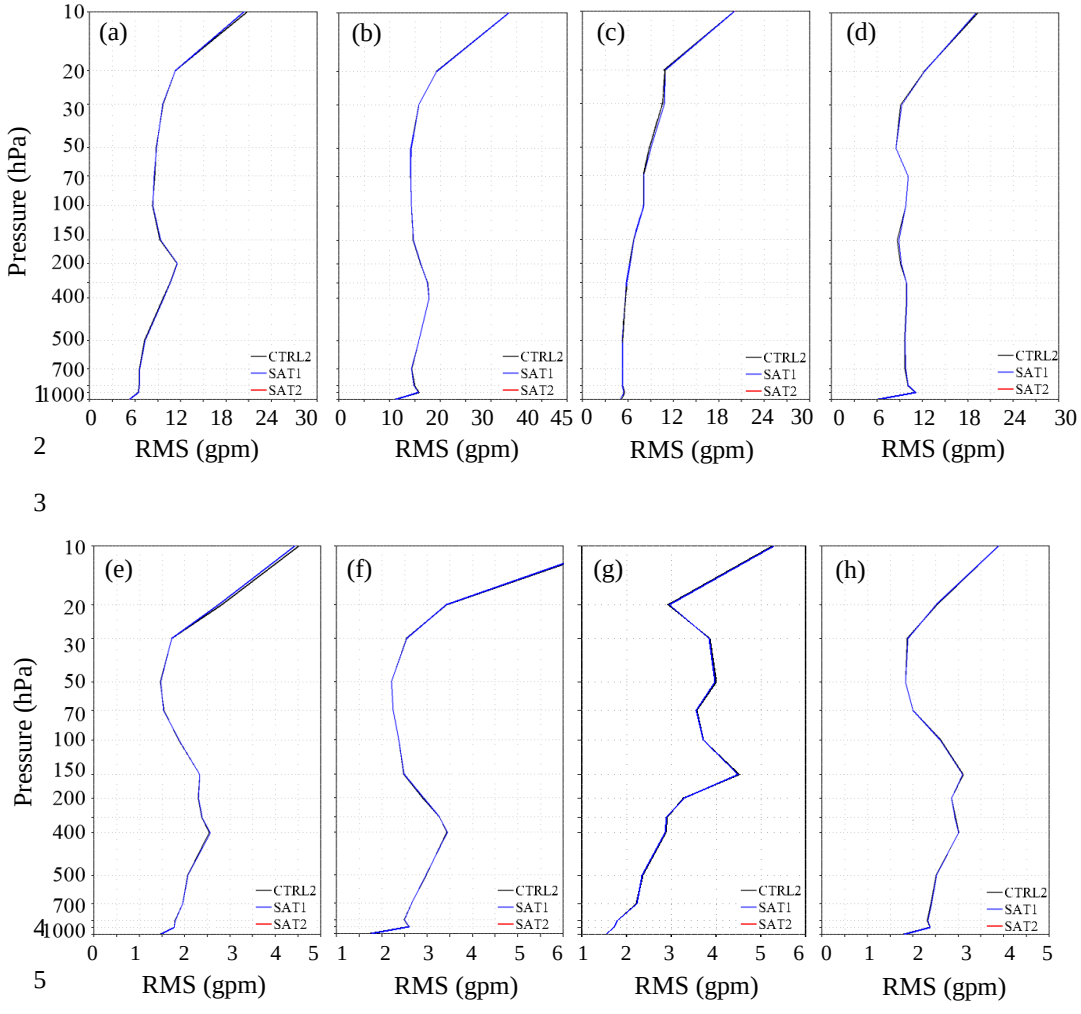

Figure 13. (a) RMS of geopotential height from the analysis field difference between CTRL2 and NCEP (black), SAT1 and NCEP (blue), SAT2 and NCEP (red) in the (a) Northern Hemisphere, (b) Southern Hemisphere, (c) Tropic and (d) East Asia during 1-27 July 2014. (e)-(h) are similar to (a)-(d) but for U wind.

Atmos. Meas. Tech. Discuss., doi:10.5194/amt-2015-361, 2016
Manuscript under review for journal Atmos. Meas. Tech.
Published: 21 January 2016

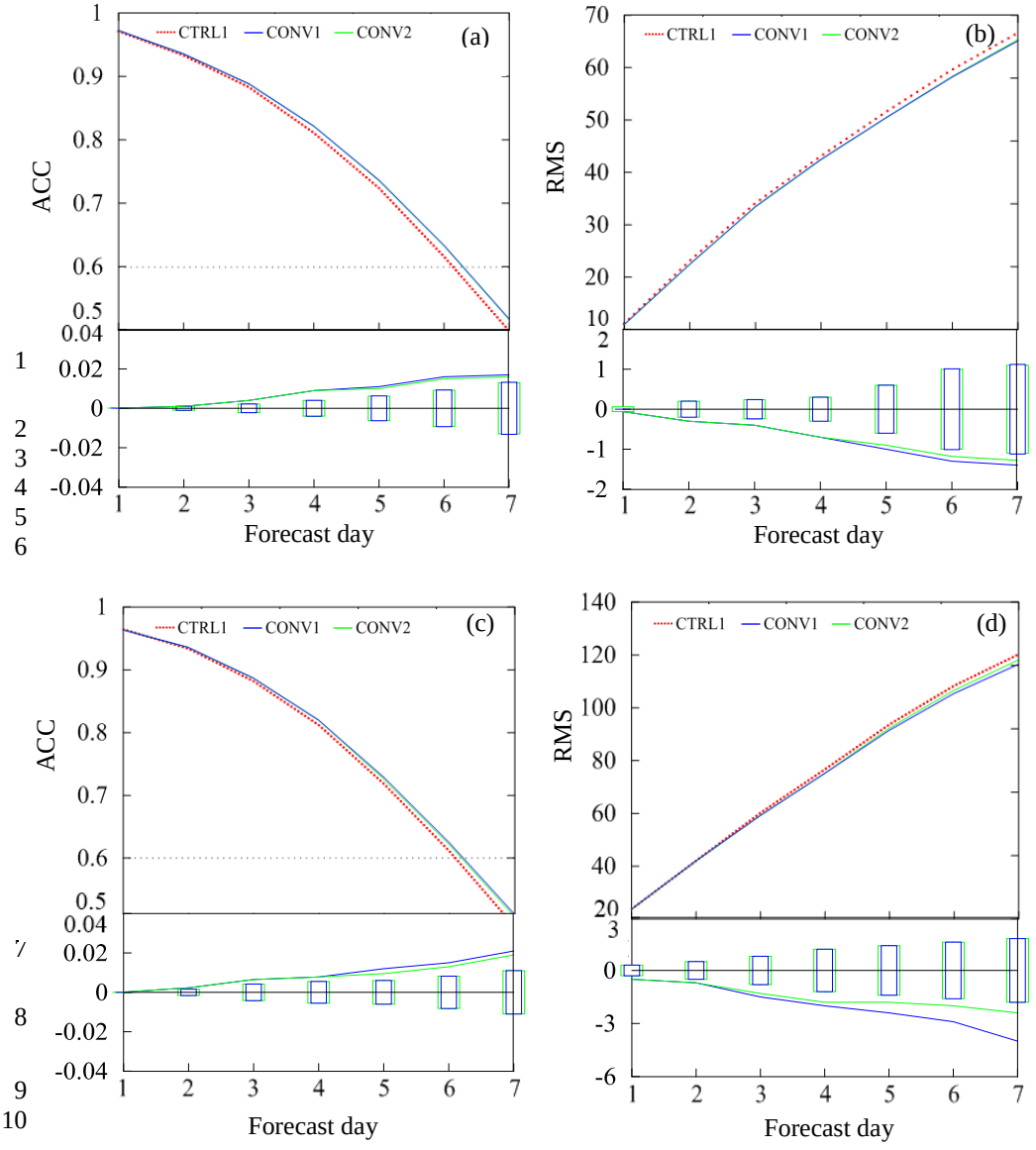

Figure 14. Mean ACC (left panels) and RMS (right panels) of 500 hPa geopotential height of CTRL1 (red dashed line), CONV1 (blue solid line), CONV2 (green solid line) experiments in (a-b) the Northern and (c-d) the Southern Hemisphere for the period from 1 to 27 July 2014. The statistical significance testing of CONV1 and CTRL1 (CONV2 and CTRL1) are shown in the lower part of each figure in blue (green). The acc and rms differences outside of outline bars are significante at the 95% confidence level.

Atmos. Meas. Tech. Discuss., doi:10.5194/amt-2015-361, 2016
Manuscript under review for journal Atmos. Meas. Tech.
Published: 21 January 2016

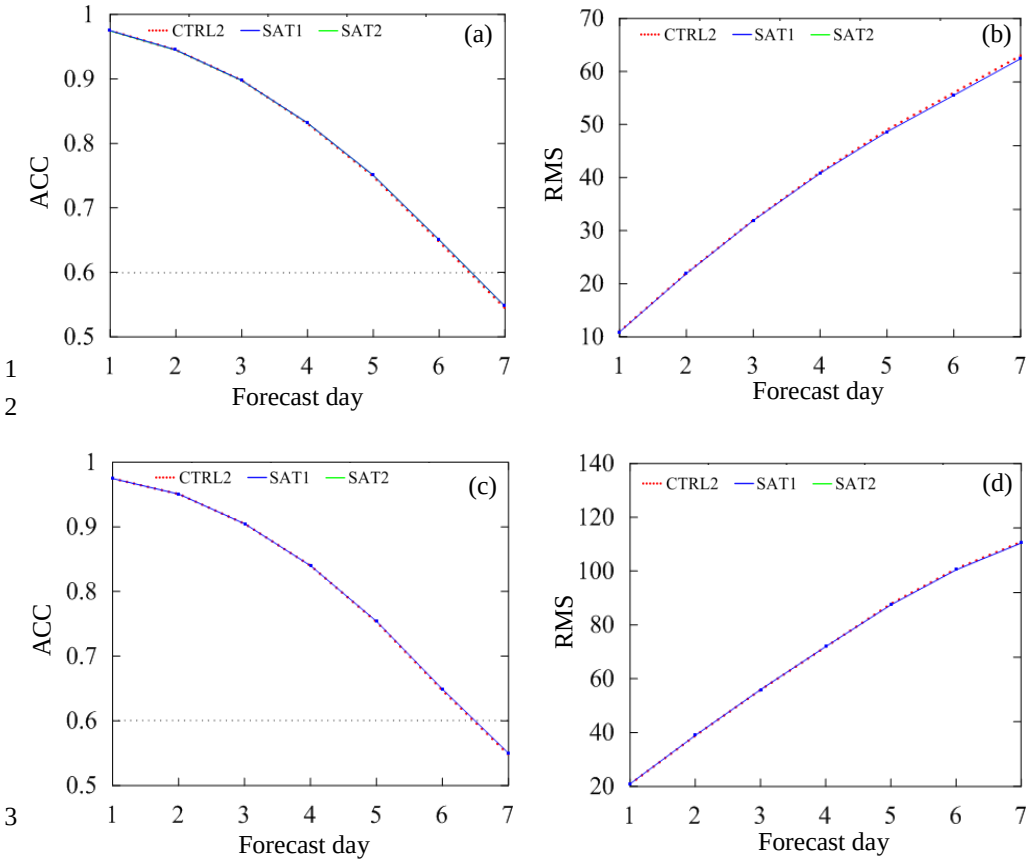

Figure 15. Mean ACC (left panels) and RMS (right panels) of 500 hPa geopotential height of CTRL2 (red dashed line), SAT1 (blue solid line) and SAT2 (green solid line) experiments in (a-b) the Northern and (c-d) the Southern Hemisphere for the period from 1 to 27 July 2014.